

Internal Waves Near Martha's Vineyard

Tom Kilpatrick
© December 14, 2005

Abstract. We analyze the internal tide observed off the southern coast of Martha's Vineyard using measurements of salinity, temperature, and current collected during field experiments from July to October, 2003. Specifically, we determine the internal tide's structure, propagation direction, and energy flux.

1. Introduction. Physical oceanography is generally concerned with the flow of momentum, mass, and heat. They pass through the turbulent boundary layer between the sea surface and atmosphere, but the process is not well understood. Consequently, the Navy funded the Coupled Boundary Layers / Air-Sea Transfer (CBLAST) project, described in [1]. The author participated in a study of the area south of Martha's Vineyard, and this study is the subject of the present paper.

What is the contribution of internal waves to this area's energy budget? This paper characterizes the internal tide—internal waves propagating at the semidiurnal frequency, $\frac{1}{12.4}$ cph—including energy flux calculations. Internal waves exist almost everywhere, propagating through the ocean depths. Although they are often invisible at the surface, they play an important role in coastal mixing and transport processes.

To study the internal tide, data was collected from the F mooring, located 10.7 km south of Martha's Vineyard; see Figure 1-1.

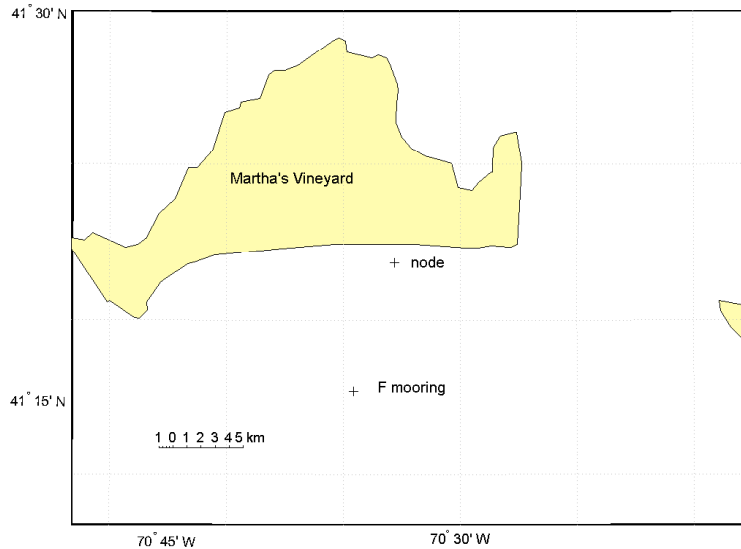


Figure 1-1. Location of F mooring. The Martha's Vineyard Coastal Observatory (MVCO) node is also shown.

Conductivity, temperature, pressure, and current measurements were recorded for a 90-day period beginning in July 2003. Sensors were placed at regular 2–3 m intervals from the surface to the ocean floor, 12 sensors in all. The recorded depth of the bottom temperature sensor was 26.9 m. There was also a bottom pressure sensor, and an Acoustic Doppler Current Profiler (ADCP), which uses sonar to measure currents through the water column.

Section 2 explains internal wave theory in detail. Section 3 describes the data processing used to analyze the internal tide, including filtering and interpolation. Section 4 describes the results obtained for direction of propagation, phase speed, and energy flux: the internal tide’s direction of propagation was variable between north and northwest, as was that of the energy flux. The energy flux’s amplitude shows that the internal tide is an insignificant part of the region’s energy budget.

2. Internal-wave theory. Internal waves arise in stratified fluids at the boundary between layers of different densities. For example, suppose that, in a two-layer fluid, a perturbation at the interface causes the lower, denser layer to rise. Gravity then supplies a downward restoring force, flattening layers of constant density, or *isopycnals*. As the upper layer’s inertia carries it past equilibrium into the lower layer, gravity again provides a hydrostatic pressure force, this time in the upward direction, causing an oscillation. This mechanism produces what is called a *mode-one internal wave*.

Mode-one internal waves are analogous to surface waves. At the surface, disturbances in sea-surface height are restored by gravity. Surface waves travel faster than internal waves, however. Large surface waves can propagate more than 100 m/s, but most internal waves have speeds of 10–50 cm/s.

The ocean is usually not a two-layer system. Generally there is a mixed surface layer, then a region of varying density, called the *pycnocline*, then the bottom layer. In the pycnocline, continuous stratification produces waves of many modes. Mode-one waves are analogous to surface waves; waves of higher modes have a more complicated structure, permitting vertical propagation of disturbances. However, on continental shelves, such as the region south of Martha’s Vineyard, mode one usually dominates over other modes.

Internal waves of all modes can be identified by their density structures. For example, at the F mooring, there were vertical displacements of several meters in mid-column isopycnals, characteristic of mode-one waves.

Internal waves can also be identified by their current structure. Progressive mode-one internal waves propagating in a single direction have the structure shown in Figure 2-1. Upward vertical displacements in the water column are in phase with bottom currents in the propagation direction, and out of phase with surface currents in that direction. (These relationships are different for waves of higher modes, standing waves, or two or more waves propagating in different directions.) The direction of propagation of the internal tide near Martha’s Vineyard was determined from this coherence between isopycnal displacements and currents.

We can gain additional insight into the current structure of internal waves by studying the governing equations of geophysical fluid dynamics, since internal waves obey these equations. Let us take v as the north-south current, positive northward; u as the east-west current, positive eastward; f as the inertial frequency, $\frac{1}{18.2}$ cph at the field site; and ρ_0 is the reference density of water. Then we have the momentum equation

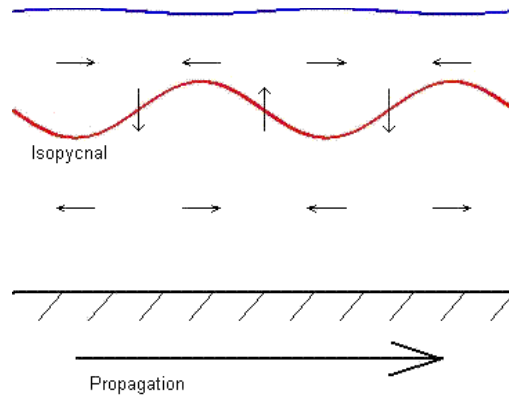


Figure 2-1. Current and isopycnal structure of a mode-one, progressive internal wave, viewed from a fixed location, as adapted from [4, p. 10].

for the x -direction, as given by Cushman-Roisin in [2, p. 43]:

$$\frac{\partial u}{\partial t} - fv = -\frac{1}{\rho_0} \frac{\partial p}{\partial x}.$$

For an internal wave propagating northward, there is no east-west pressure gradient. Thus $\frac{\partial p}{\partial x} = 0$, and the east-west momentum equation becomes

$$\frac{\partial u}{\partial t} - fv = 0.$$

Assuming the wave form $e^{-i\sigma t}$ where σ is the internal wave frequency, we obtain the solutions

$$\begin{aligned} v &= v_0 e^{-i\sigma t}, \\ u &= \frac{f}{\sigma} v_0 e^{-i(\sigma t - \frac{\pi}{2})}. \end{aligned} \quad (2-1)$$

So we expect that v “leads” u by a phase angle of $\pi/2$ radians or 90° , and that the magnitude of u is smaller than v by $|f/\sigma|$. Viewed from above, the current vector (u, v) should trace an ellipse, as described in [3, p. 132]. In addition, the surface and bottom currents ought to be 180° out of phase, as shown in Figure 2-1.

We restrict our analysis of internal waves to the internal tide. We refer to the *internal tide* as internal waves in a narrow frequency band centered on the semidiurnal, or M_2 frequency, $\frac{1}{14.5}$ to $\frac{1}{11}$ cph.

There is a subtle distinction between the surface tide and the internal tide. Surface tides are caused by the moon: its gravitational pull causes water to slosh around the surface of the Earth at the M_2 frequency. This tide is the familiar one.

The internal tide is thought to be caused by the surface tide forcing water over the bottom topography of the ocean floor. The internal tide is ubiquitous: the internal wave spectrum shows how much energy is contained in waves at each frequency; it shows a peak at the M_2 frequency almost everywhere in the ocean, according to [3, p. 305].

Note that the internal tide refers to waves. Like any water waves, internal waves are dispersive. Thus an internal wave of angular frequency ω and wave number k has phase speed c_p , given by

$$c_p = \frac{\omega}{k}.$$

Phase speed is the speed of lines of constant phase. For example, in surface waves, c_p is the speed at which wave crests travel. The phase speed of internal waves depends on the stratification frequency N , to be explained in Section 3, water depth H , wave mode n , inertial frequency f , and wave frequency σ , according to the formula

$$c_p = \frac{NH}{n\pi} \frac{1}{1 - (f/\sigma)^2}. \quad (2-2)$$

After the internal tide has been identified from its current and isopycnal structure, we can calculate the energy flux. Is this quantity significant when compared to other sources of energy in a region, such as wind and sunlight? The energy flux density vector \vec{F} is defined as the time average, indicated by an overbar, of the product of the perturbation pressure p' , and the perturbation velocity \vec{s} , as defined in [3, p. 141]:

$$\vec{F} = \overline{p' \vec{s}}. \quad (2-3)$$

The vector \vec{F} is the mean energy flux of the wave. The quantities p' and \vec{s} are defined in Section 3, but note that the perturbation velocity \vec{s} is not the phase velocity c_p . For example, in surface waves, \vec{s} is the water velocity measured at a fixed point; it changes as a surface wave passes.

3. Data Processing. The internal tide cannot be identified directly from the time-series recorded at the mooring. The raw data only includes temperature, salinity, pressure, and current measurements. However, to calculate direction of propagation, energy flux, and phase speed, we need to know isopycnal displacements ξ , perturbation velocity \vec{s} , and stratification frequency N . Thus the time series from the mooring were filtered and converted into ξ , \vec{s} , and N .

The mid-column isopycnal displacement ξ was computed first. When a mode-one internal wave passes through stratified water, it vertically displaces density isopycnals, as shown in Figure 2-1.

Although water density is a nonlinear function of salinity, temperature, and pressure, seawater density is typically a strong function of temperature. Salinity and pressure affect the density, but much less than temperature. Thus, in stratified seawater, layers of constant temperature are equivalent to density isopycnals. For simplicity, ξ was calculated from the temperature data.

To calculate ξ , the water column was first assumed to be temperature-stratified, with warmer water near the surface and colder water near the ocean floor. Then, temperature data were “low-passed,” or filtered to remove variation with frequencies higher than $\frac{1}{33}$ cph, including the M_2 frequency. This filtering isolated the low frequency band, providing a baseline from which ξ could be calculated using the raw temperature time series. Displacements ξ calculated this way only contain variation at high frequencies, or the range above $\frac{1}{33}$ cph.

This time series of ξ is sufficient for computing the direction of propagation, but for the energy flux, we need the density perturbation ρ' , closely related to ξ . We calculate ρ by using our density-temperature relationship, $\rho = \rho(T)$. We calculate $\rho'(z, t)$ from ρ and the “low-passed” density ρ_{lp} :

$$\rho'(z, t) = \rho - \rho_{lp}.$$

The density perturbation is used to calculate the pressure perturbation p' , as described by Nash in [5, p. 1122]:

$$p'(z, t) = p'_{\text{surf}}(t) + \int_z^0 \rho'(\hat{z}, t) g d\hat{z}. \quad (3-1)$$

The perturbation surface pressure p'_{surf} is not measured, but is inferred from the requirement that the depth-averaged pressure perturbation vanishes when integrated over the water depth H :

$$\frac{1}{H} \int_{-H}^0 p'(z, t) dz = 0.$$

We now have the pressure perturbation p' required to calculate the energy flux \vec{F} , given by Equation (2-3).

We still need to find the perturbation velocity \vec{s}' . At both locations, an ADCP measured currents u and v . However, the current structure of the internal tide was difficult to identify from the unprocessed data because the surface tide dominates. Consequently, we only consider the perturbation velocity \vec{s}' for our analysis. The vector \vec{s}' has scalar components (u', v') . The currents u' and v' are obtained by removing low-frequency variation from u and v , and then removing the vertical mean of the remaining “high-passed” currents, \bar{u}_{hp} and \bar{v}_{hp} :

$$u' = u - u_{\text{lp}} - \bar{u}_{\text{hp}}, \quad (3-2)$$

$$v' = v - v_{\text{lp}} - \bar{v}_{\text{hp}}. \quad (3-3)$$

By definition, current perturbations also have vanishing temporal and depth averages:

$$\frac{1}{H} \int_{-H}^0 \vec{s}' dz = 0.$$

Finally, we compute the *stratification frequency*, or Brunt–Väisälä frequency, N . It is a measure of the change in water density with depth, and is given by the formula

$$N^2 = -\frac{g}{\rho_0} \frac{d\rho}{dz}.$$

Thus the stratification frequency is a function of $\frac{d\rho}{dz}$, the rate of change of density with depth. In regions of high stratification, N is high; in regions of low stratification, N is low.

Stratification frequency is often approximated from the readings at just the top and bottom sensors. Figure 3-1 shows N , calculated in this manner at the F mooring; we get a rough idea of the stratification. Notice that the stratification breaks down during the second half of the deployment.

The relationship between density and stratification frequency at the F mooring is shown in Figure 3-2. The left diagram shows a mean depth profile of density: we see a well-mixed surface layer roughly 6 m thick, a pycnocline of 14 m, and a mixed bottom layer of about 5 m. The right diagram shows a mean depth profile of N . The data in both diagrams are averaged over the first half of the deployment, July 16 to August 27.

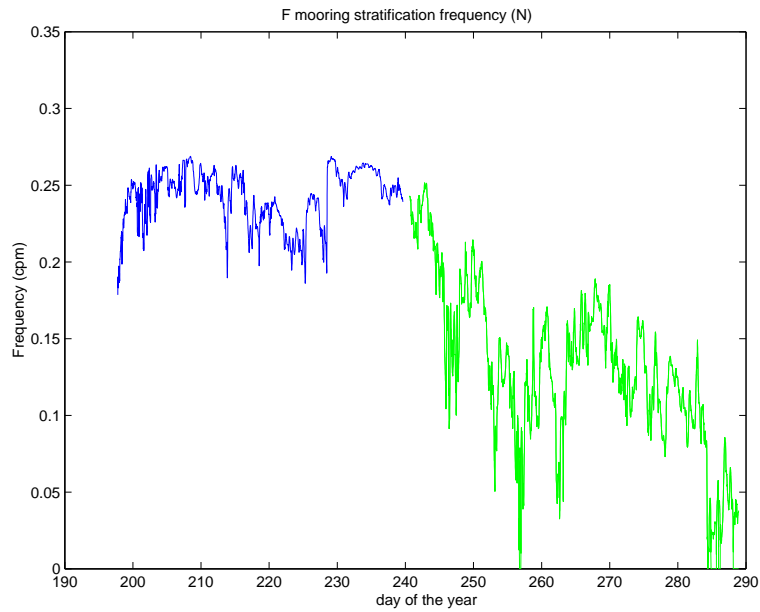


Figure 3-1. Stratification frequency at the F mooring.

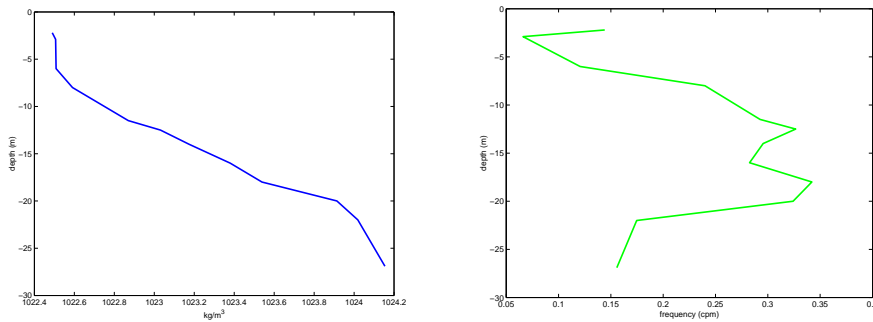


Figure 3-2. Left: Mean density profile. Right: Mean stratification frequency profile.

4. Results. If the internal tide is present at the F mooring, then it should be visible in the time-series of u' , v' , and ξ . Once we establish that the internal tide exists, we can characterize its direction of propagation, phase speed, and energy flux.

If we examine surface and bottom currents at the F mooring, we see they are nearly 180° out of phase, just as we expect from Figure 2-1. After band-averaging for frequencies between $\frac{1}{11}$ cph and $\frac{1}{14.5}$ cph over the first half of the deployment, we observe that surface and bottom u' currents are 166° out of phase with a coherence-squared of 0.85, and surface and bottom v' currents are 174° out of phase with a coherence-squared of 0.75. Coherence-squared measures the dependence of signals: independent signals have a coherence-squared of zero; signals oscillating at the same frequency have a coherence-squared of 1.

The power spectra for u' and v' reveal a peak of energy at the M_2 frequency, as we expect. However, we also notice a peak at the inertial frequency, $\frac{1}{18.2}$ cph, in the surface

currents, as shown in Figure 4-1. The inertial peaks are likely due to wind stress. The power spectrum for the isopycnal displacement ξ shows peaks near both the inertial and M_2 frequencies, and several smaller peaks.

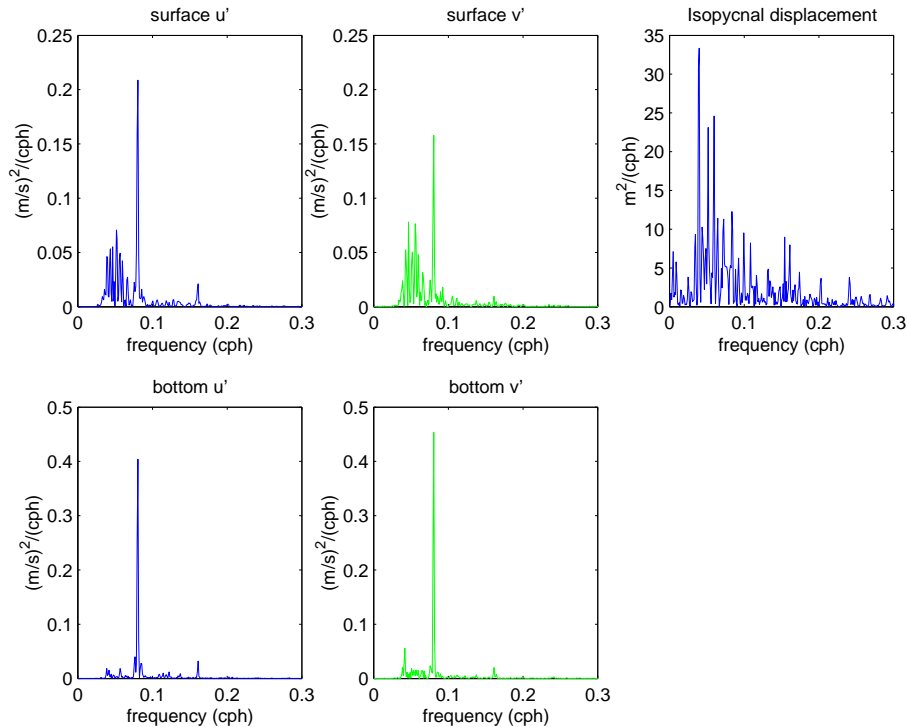


Figure 4-1. Power spectra of u' , v' , and ξ at F mooring.

Equation (2-1) suggests that v' leads u' by 90° for a northward-propagating internal wave, and we observed this behavior at the F mooring; see Figure 4-2. After band-averaging for the M_2 frequency, $\frac{1}{14.5}$ cph to $\frac{1}{11}$ cph, over the first half of the deployment, we observe that bottom v' leads bottom u' by 94° with a coherence-squared of 0.88. At the surface, v' leads by 102° with a coherence-squared of 0.86.

Now that we have observed the expected phase relationships between u' and v' , and the power spectra for u' , v' , and ξ , we can characterize the internal tide in more detail.

First, we calculate the direction of propagation. From u' , v' , and ξ , we determine the direction by analyzing the relationships in Figure 2-1. We only consider bottom currents from the first half of the deployment. We do not consider surface currents because of the inertial energy they contain; see Figure 4-1. We do not consider the second half of the deployment because stratification breaks down there, making it difficult to interpolate ξ ; see Figure 3-1.

We observe that v' trails ξ by 18° and u' trails ξ by 129° . To determine the direction of propagation we rotate the assumed (u, v) -axes counterclockwise until currents in the direction of the new v -axis are in phase with ξ . The axes align after 18° of rotation, the lag between v' and ξ . In other words, the mean direction of the internal tide was 18° west of north, roughly north-northwest.

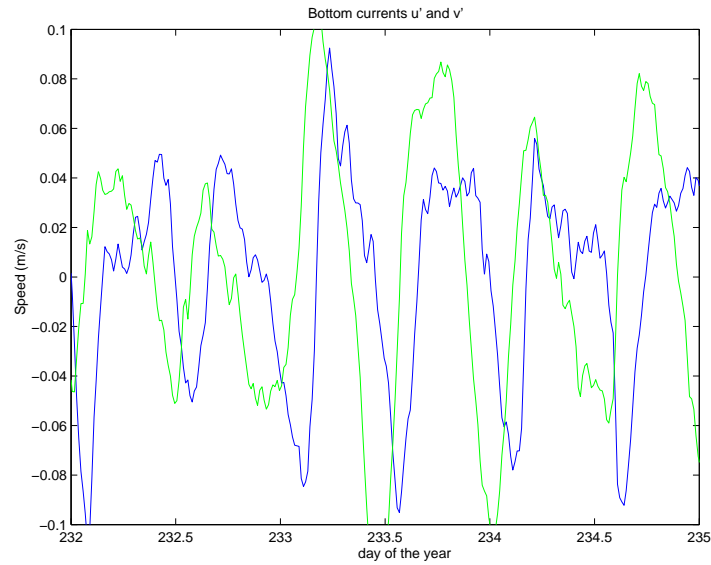


Figure 4-2. Phase relationship between bottom u' , black, and bottom v' , grey, at F mooring.

Coherence-squared between bottom currents and ξ over the first half of the deployment was low: 0.07 between v' and ξ , 0.05 between u' and ξ . Figure 4-3 shows how this

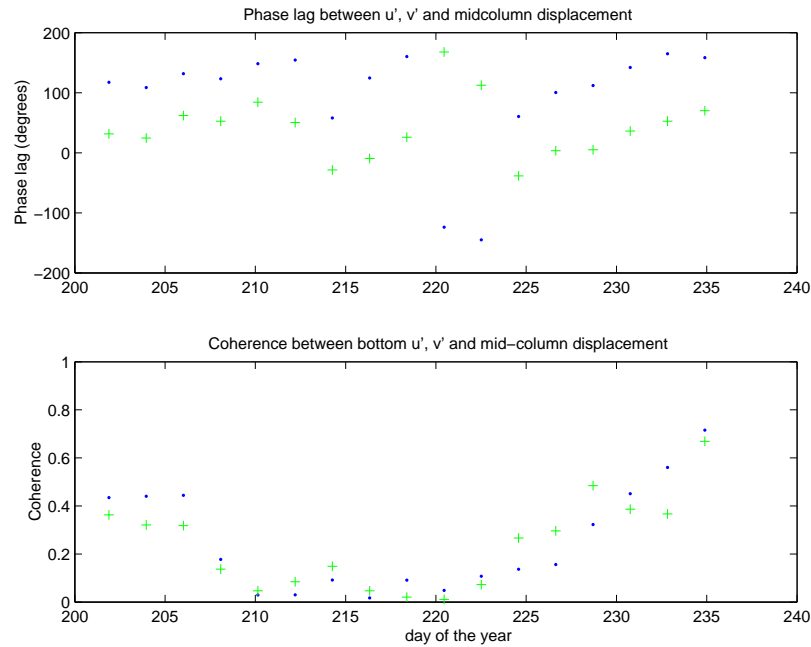


Figure 4-3. Top: propagation direction. Bottom: coherence between u' and ξ , and v' and ξ . Dots represent u' ; pluses represent v' .

coherence-squared, and propagation direction, vary over the first half of the deployment.

A positive phase lag θ° between v' and ξ means that the internal tide propagates at θ° west of north. Each point represents an 8-day average.

The direction of propagation varies between north and northwest during periods when coherence is “high,” which we take as more than 0.2; this value of significance was estimated, not statistically determined. The direction of propagation was expected to be steady, so this result is a surprise.

Next, we calculate the phase speed. We can predict the phase speed of the internal tide during the first half of the deployment, since we know that $N = 0.026$ rad/s, $H = 27$ m, $n = 1$, $f = \frac{1}{18.2}$ cph, and $\sigma = \frac{1}{12.4}$ cph. Equation (2-2) yields a phase speed of 0.42 m/s.

The phase speed c_p was also measured from the phase lag between bottom currents at the F mooring and a near-shore mooring shown in Figure 1-1, the Martha's Vineyard Coastal Observatory (MVCO) node. If ΔS is the separation, 9.7 km, between the two moorings, ϕ_{lag} is the phase lag between bottom currents, the angle θ is the separation, 35° on average, between the line of propagation and the line connecting the two moorings, and $\frac{1}{M_2}$ is the period, 12.4 hours, of the M_2 frequency, then c_p is given by the formula

$$c_p = \frac{\Delta S \cos \theta}{\frac{\phi_{\text{lag}}}{360^\circ} \frac{1}{M_2}}. \quad (4-1)$$

Ensemble-averaging bottom currents, we determine that v' at the F mooring leads v' at the MVCO node by 188° at the M_2 frequency; see Figure 4-4. Equation (4-1) yields $c_p = 0.34$ m/s for the internal tide.

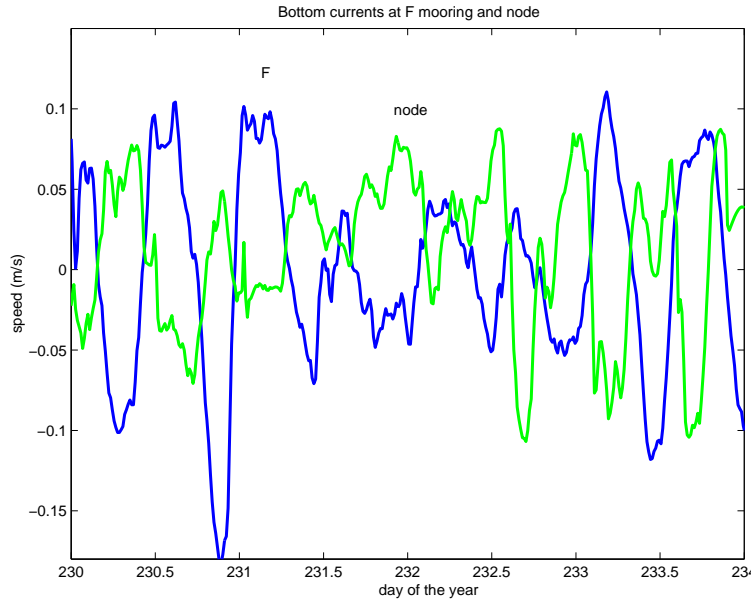


Figure 4-4. Bottom v' at F mooring and MVCO node, August 18 through August 20.

We also determine c_p from the phase lag between isopycnal displacements at the two locations. We observe that ξ at the F mooring leads ξ at the MVCO node by 312° ; see Figure 4-5. Note that the phase lag is not as clear as in Figure 4-4. Based on isopycnal displacements, c_p is 0.21 m/s.

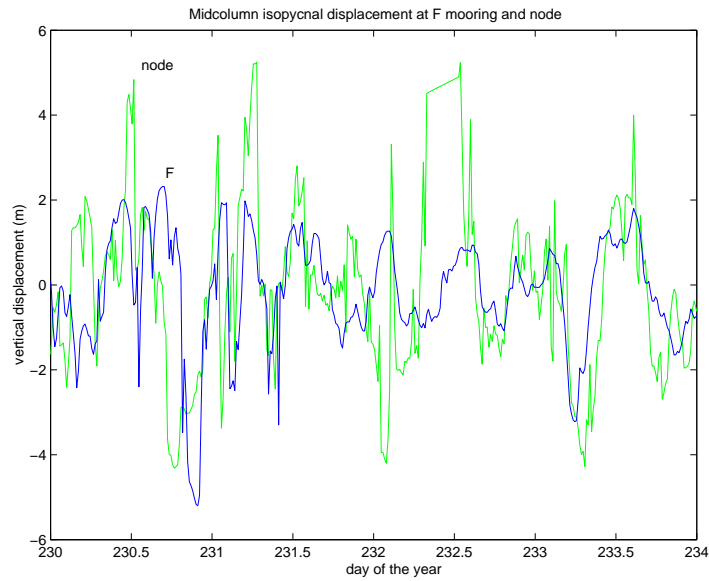


Figure 4-5. Mid-column isopycnal displacements ξ at F mooring and MVCO node.

The wavelength λ of the internal tide off of Martha's Vineyard is c_p/σ , or 15.2 km, if we use c_p as calculated from bottom currents.

Finally, we determine the energy flux, using Equation (2-3), Equation (3-1), Equation (3-2), and Equation (3-3). After filtering the pressure perturbation and current data for the M_2 band, we calculate the average energy flux over the first deployment to be 0.51 W/m, and average direction of propagation to be 57° west of north. However, the amplitude and propagation direction vary; see Figure 4-6.

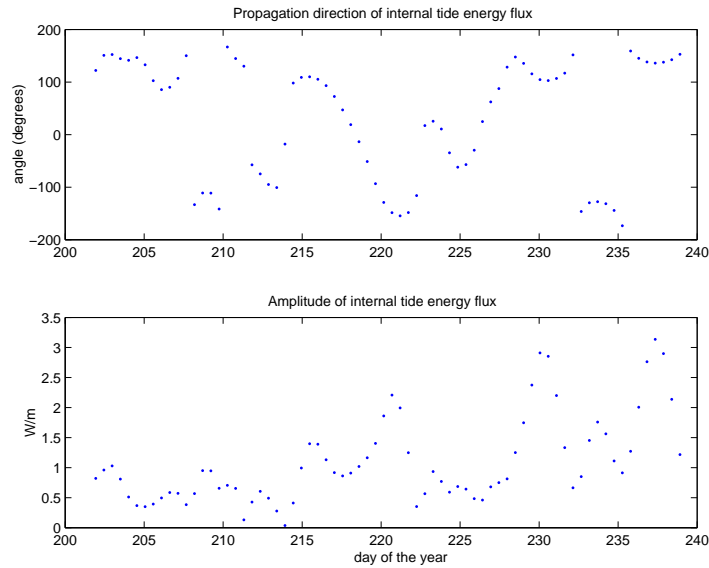


Figure 4-6. Top: propagation direction. Bottom: amplitude of internal tide energy flux.

In the figure, each point represents a 12.4-hour average. A propagation direction of 0° is due east, and counterclockwise rotation is considered positive. The amplitude appears to grow over the deployment. The units are W/m instead of W/m^2 because the flux vector was vertically integrated.

We can compare the energy flux of the internal tide to other sources of energy by considering the energy per unit area it supplies to the region south of Martha's Vineyard. The south coast of Martha's Vineyard is 20 km long, perpendicular to the energy flux vector, so the internal tide supplies 10 kW to the region. That region spans 200 km^2 , namely, 20 km of coast times 10 km to the F mooring; so the energy is spread over 200 km^2 of water. The flux equals $5 \times 10^{-5} \text{ W}/\text{m}^2$, negligible compared to other sources like the sun, which can radiate $100 \text{ W}/\text{m}^2$.

The calculated energy flux could be smaller than what is actually being transported to Martha's Vineyard if the internal tide reflects off the ocean floor, back out to sea. If this reflection occurs, then the flux of energy moving off-shore would reduce the calculated values for on-shore propagation of energy.

ACKNOWLEDGEMENTS

The author thanks his advisor, Jim Lerczak of Physical Oceanography, for all his help. The author also thanks Bob Weller of Physical Oceanography and John Trowbridge of Applied Ocean Physics and Engineering for the CBLAST data, and the Summer Student Fellow program for the opportunity to study at Woods Hole. Lastly, the author thanks Steven Kleiman and Susan Ruff for helping to revise this paper.

REFERENCES

- [1] "Coupled Boundary Layers/Air-Sea Transfer (CBLAST) Defense Research Initiative," <http://www.whoi.edu/science/AOPE/dept/CBLASTmain.html>, accessed Sept 2005.
- [2] Cushman-Roisin, Benoit, "Introduction to Geophysical Fluid Dynamics," Prentice-Hall, 1994.
- [3] Gill, A.E., "Atmosphere-Ocean Dynamics," Academic Press, 1982.
- [4] Lerczak, J., *Internal Waves in the Ocean: From Internal Tides to Internal Surf*, presentation at WHOI, 28 July 2005.
- [5] Nash, J.D., Kunze, E., Toole, J.M., and Schmitt, R.W., *Internal Tide Reflection and Turbulent Mixing on the Continental Slope*, *J. Phys. Oceanogr.* **34** (2004), 1122–1125.